



A probabilistic modeling and simulation framework for power grid flood risk assessment

Panagiotis Asaridis ^{a,*}, Daniela Molinari ^a, Francesco Di Maio ^b, Francesco Ballio ^a, Enrico Zio ^{b,c}

^a Department of Civil and Environmental Engineering, Politecnico di Milano, Milan, Italy

^b Department of Energy, Politecnico di Milano, Milan, Italy

^c Mines Paris-PSL, Centre de Recherche sur les Risques et les Crises (CRC), Sophia Antipolis, France



ARTICLE INFO

Keywords:

Power grids

Flood risk

Risk assessment

ABSTRACT

Floods can cause power outages with widespread impacts on socio-economic activities dependent on electricity for their functioning. Effective flood risk management requires comprehensive damage assessment, yet methodologies to estimate the entire range of expected damages are lacking. This paper presents a new modeling and simulation probabilistic framework for the assessment of damages to power grids exposed to floods. The framework combines modeling tools and approaches from engineering, economics and sociology, namely a flood inundation model to generate stochastic hazard scenarios, fragility curves to describe the stochastic failure process of components in the power grid conditioned to the hazard, a simulation-based model to analyze the power flow, and a socio-economic model to characterize the customers connected to the power grid. Consequently, the framework enables: (i) considering the stochastic magnitude and frequency of floods, (ii) evaluating the vulnerability of power grids components, (iii) estimating their spatio-temporal probabilities of failure, (iv) analyzing the cascading effects across power transmission and distribution networks, and (v) assessing the impact of power outages on the final customers and their likelihood. A synthetic case study is worked out by adapting the IEEE 14 power grid benchmark to the Italian context, proving how the framework allows the identification of the most critical components for the security of power supply during flooding. The outcomes from the implementation of the framework can support civil protection agencies and grid operators in the decision on pre- and post-disruption mitigation strategies, so to guarantee public safety, secure power supply and ensure financial well-being.

1. Introduction

Power grids are critical infrastructures (CIs) that must provide safe, secure and reliable supply of electricity. Natural hazards are primary causes of power outages around the world [1,2]. In particular, floods pose significant threat of outages in terms of magnitude and duration [3]. Indeed, recovery from flooding may be long due to the perduration of its damage. For example, thousands of people experienced power outages in the 2021 floods in Germany, Belgium and the Netherlands, remaining without access to electricity from a few weeks to a month, before electricity supply was finally restored [4]. Furthermore, there is the potential danger of escalation of

* Corresponding author.

E-mail address: panagiotis.asaridis@polimi.it (P. Asaridis).

damage to other CIs (i.e., transportation, communication, etc.) [5,6].

Current flood risk assessment generally neglects, or estimates with over-simplified assumptions and tools, the damage to power grids [7]. This is due to (i) lack of knowledge on damage mechanisms [8], (ii) scarcity of data to validate and calibrate the models [9], and (iii) the inherent structural and dynamic complexity of the power grid, that calls for an integrated framework of different types of analysis and modeling methods [10].

Flood damage is typically classified into direct and indirect damage, whose assessment requires different modeling approaches. Direct damage concerns people, properties, or any other object when in physical contact with floodwater, whereas indirect damage is induced by the direct damage, not necessarily at the same time and outside the inundation area. Both types are further divided into tangible and intangible damages, depending on whether they can or not be quantified in monetary terms [11,12]. Still, among different disciplines, there is not a clear, univocal classification of flood impact. For example, clean-up costs may be considered direct or

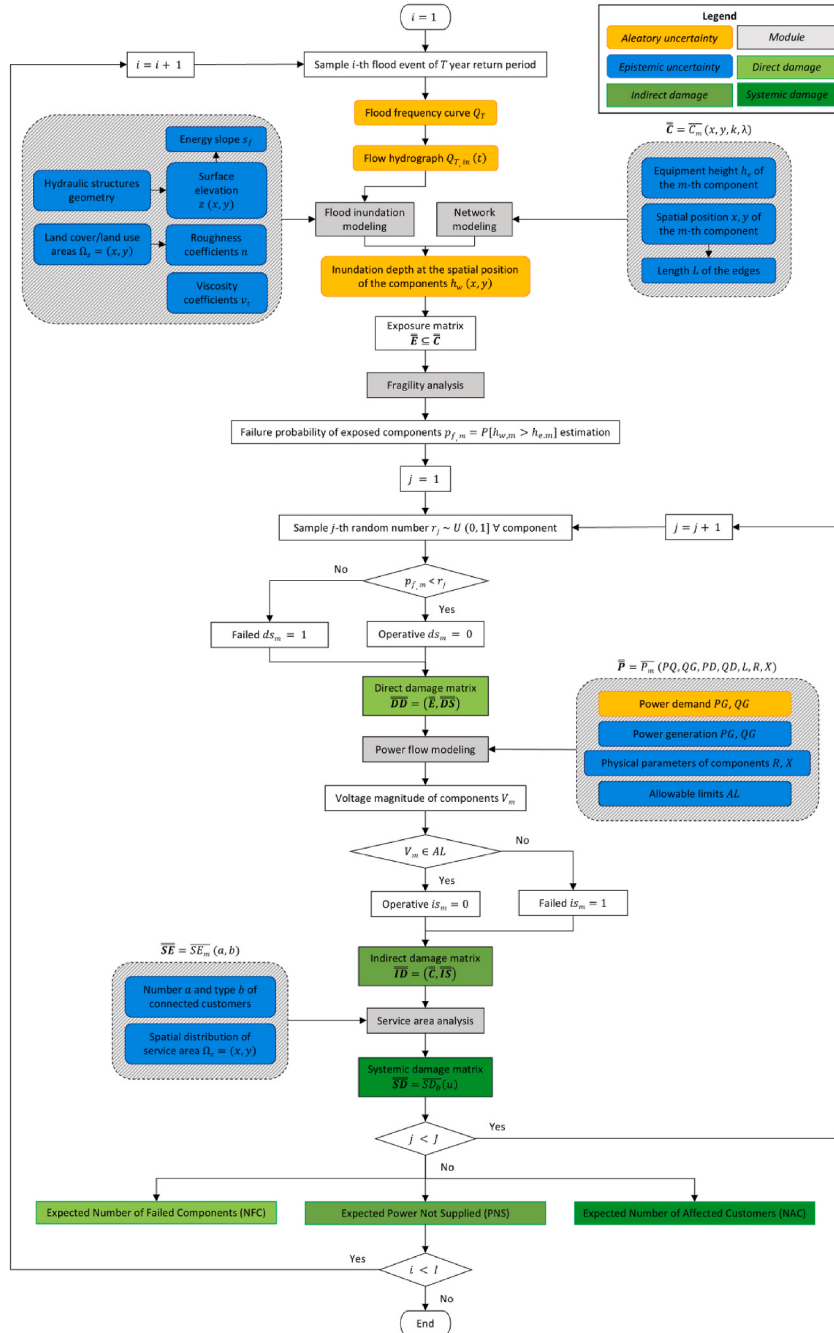


Fig. 1. The flowchart of the probabilistic modeling and simulation framework.

indirect. Indirect damage can be further distinguished among systemic, functional, economic, etc.

According to the classification adopted by Ref. [13], flooding of power grids can lead to three kinds of damage.

- Direct: functional failures of components, due to physical contact with floodwater or flood-induced riverbank erosion;
- Indirect: loss of network functionality as an indirect effect of the direct damage to the network components;
- Systemic: disruption of economic and social activities that depend on power supply.

Despite significant recent efforts to better understand and quantify the direct [14,50,51], indirect [14–20] and systemic [5,21–30] damages, to our knowledge there is not yet a consolidated framework for a comprehensive modeling, simulation and analysis of flood damage to power grids, capable of probabilistically capturing the stochasticity of the full range of damaging phenomena, their cascading effects and the evaluation of their socio-economic impacts. For example, Espinoza et al. [14] evaluates power plants and substations failure probabilities by means of rainfall-based fragility curves and assesses the power network performance with power flow simulations, but not its impact on end-users; Karagiannis et al. [23] evaluates the impact of power outages on commercial and industrial customers using Voronoi diagrams to estimate the number of people affected, assuming that operators curtail the load of the substations located in the flood-affected areas rather than modeling their failures; Koks et al. [24], again using Voronoi diagrams, assesses the impact of power supply disruption on businesses, industries and agriculture, without relying on a mechanistic model of the power grid. The available methodologies struggle to make the transition from one type of damage to another, and as a consequence, they tend to primarily focus on one particular type, or perhaps two, at a time [13].

In this paper, we propose a probabilistic modeling and simulation framework for the comprehensive assessment of the risk to power grids due to flooding, addressing the full spectrum of expected damages. In the framework, we combine several modeling tools and approaches from the disciplines of engineering, economics and sociology, namely: a flood inundation model to generate stochastic hazard scenarios, fragility curves to quantify the power grid components failure probabilities conditional on the hazard, a simulation-based model to analyze the power flow (see Ref. [14]) and a socio-economic model to describe the impacts on the customers connected to the grid (as proposed by Ref. [24]).

For illustrating the modeling and simulation probabilistic framework, we have created a synthetic case study derived from the Institute of Electrical and Electronics Engineers (IEEE) 14 power grid benchmark [31], in which the river crossing (i.e., hazard source), the generation, transmission and distribution systems and components (i.e., power grid elements), and the connected socio-economic activities (i.e., customer categories) are spatially distributed. The case study demonstrates that the proposed framework allows performing probabilistic damage assessments in relation to flooding events of different frequency and magnitude to identify critical components of the power grid.

The remainder of the paper is organized as follows. Section 2 introduces the modeling and simulation framework, and describes the models therein. In Section 3, the synthetic case study is described, and the framework is applied to it. In Section 4, the results of the analysis are presented. In Section 5, a critical discussion of the results is provided. In Section 6, concluding remarks are given.

2. The probabilistic modeling and simulation framework

The framework, shown in Fig. 1, is operationalized within a double-loop Monte Carlo (MC) simulation. This entails sampling I random hazard scenarios of river flooding simulated by a flood inundation model whose effects are assessed by modeling the stochastic failures of M assets, conditioned on their fragility to the hazard occurred, and running a power flow model of the network, to which different types of customers are connected. For the probabilistic assessment of the direct, indirect and systemic damages, we estimate J times the health state (failure or operational) of the network components exposed to the hazard, where for each time we evaluate the resulting voltage profile of the power transmission and distribution networks, and assess the impact of power supply disruptions on the end-users in terms of some probabilistic metrics, one for each of the three types of damage. Specifically, we calculate the expected Number of Failed Components (NFC) for the direct damage, the expected Power Not Supplied (PNS) for the indirect damage and the expected Number of residential, commercial, industrial and agricultural Customers Affected by power interruptions (NAC) for the systemic damage.

2.1. Framework

Each MC simulation requires in input.

- the magnitude of the flood event, in terms of the annual peak discharge Q_T of the river, and the associated frequency, in terms of the annual exceedance probability $p_e = P[Q \geq Q_T] = 1/T$ (i.e., the probability in a given year that a flood event will reach or exceed Q_T), estimated by a flood frequency curve;
- the corresponding inflow rate over time $Q_{T,in}(t)$ of the water entering the river, estimated by a hydrograph, and the friction slope s_f (i.e., slope of the energy grade line) of the river near the end point, according to which the outflow rate $Q_{T,out}(t)$ is estimated, representing the upstream and downstream boundary conditions of the flow area, respectively;
- the geomorphology of the river and of the affected area (i.e., the terrain), described by means of a Digital Terrain Model (DTM) that defines the surface elevation z over the set of spatial cartesian coordinates $\Omega = (x,y) \subset \mathbb{R}^2$, also including the geometry of hydraulic

structures (e.g., levees, bridges), and by the spatial distribution of the surface roughness, on which depends the resistance to flood flow in river channels and floodplains, expressed by the n Manning's roughness coefficients;

- the eddy viscosity v_t , that models the turbulent flow motion;
- the list of the characteristics of the components of the power grid (i.e., the network topology), summarized in the “components” matrix $\bar{\bar{C}}$, whose row $\bar{C}_m(x, y, k, \lambda)$ defines, for the m -th component, $m = 1, \dots, M$, the location (x, y) , according to which the length L of edges between the nodes is estimated, its type $k = 1, \dots, K$ (e.g., cabins, poles, towers) and the subsystem $\lambda = 1, \dots, \Lambda$ to which the specific component type belongs to (e.g., transmission, distribution);
- the fragility curve $FC_{k\lambda}$ of each k -th type of component belonging to the λ -th subsystem of the network as a function of the equipment elevation h_e , estimated on the basis of the physical vulnerability characteristics;
- the power generation and demand profile for each m -th component of the power network, as well as the physical parameters, all summarized in the “power” matrix $\bar{\bar{P}}$, whose m -th row is $\bar{P}_m(PG, QG, PD, QD, L, R, X)$, where PG and QG are the active and reactive power therein (eventually) generated, respectively, PD and QD the active and reactive power therein (eventually) demanded, respectively, and L, R and X the lumped parameters modeling the length, resistance and reactance, respectively;
- the number a of customers, for each type $b = 1, \dots, B$ (e.g., residential, commercial, industrial), that are connected to the same m -th components. These are, therefore, grouped in $Z \subseteq M$ service areas $\Omega = \{\Omega_1, \dots, \Omega_z, \dots, \Omega_Z\}$, all summarized in the “socio-economic” matrix $\bar{\bar{S}} E$, whose m -th row is $\bar{S}E_m(a, b)$. In doing so, we assume that only one category of customers can be connected to a component.

The pseudocode of the probabilistic modeling and simulation framework is as follows.

1. For $i = 1$ to I :
 - 1.1. Sample a random return period T (years) of the i -th flood event.
 - 1.2. The upstream boundary condition of the flow area, i.e., the inflow rate $Q_{T,m}(t)$, is fed to the flood inundation model, as described in Section 2.2.1, that runs to calculate the inundation depth (i.e., hazard intensity variable) in the spatial domain $h_w(x, y)$ for the triggering hazard scenario with return time T .
 - 1.3. The exposure of components to flood is calculated and, then, stored in the “exposure” matrix $\bar{\bar{E}} \subseteq \bar{\bar{C}}$: the m -th component \bar{C}_m located in (x, y) is “exposed” if $h_{w,m}(x, y) > 0$.
 - 1.4. The fragility of the power grid components, as described in Section 2.2.3, is analyzed to estimate the probability $p_{f,m}$ that the m -th component fails due to the inundation depth $h_{w,m}$ of the considered flood event it is exposed to (i.e., the direct damage), calculated as $p_{f,m} = P[h_{w,m} > h_{e,m}]$, with $h_{e,m}$ being the equipment elevation of the exposed component.
 - 1.5 For $j = 1$ to J :
 - 1.5.1 Sample a random number r_j for each m -th exposed component from a uniform distribution $U(0, 1)$: if the failure probability $p_{f,m}|h_w$ of the m -th component when exposed to a floodwater level h_w exceeds r_j , the m -th component fails, otherwise not, so that the m -th component health state is defined as $ds_m = \{0, 1\}$ (e.g., operative (0), failed (1)):
 - 1.5.1.1 if $p_{f,m} > r_j$, the m -th exposed component fails due to the flood event so that $ds_m = 1$ for each failed component;
 - 1.5.1.2 if $p_{f,m} < r_j$, the m -th exposed component withstands the event so that $ds_m = 0$ for each operative component.
 - 1.5.2 Results are collected in the “direct damage” matrix $\bar{\bar{D}} D = (\bar{\bar{E}}, \bar{\bar{D}} S)$, where the vector $\bar{D}S$ summarizes the ds_m operational states of the m -th exposed components due to the direct damage.
 - 1.5.3 The power flow model is fed with the $\bar{\bar{D}} D$ matrix: the m -th exposed component with direct operational state $ds_m = 1$ is assumed “failed” and disconnected from the network.
 - 1.5.4 The power flow model is run to calculate the voltage magnitude V_m in each m -th node, stored in the “voltage” vector \bar{V} , and the power outage (i.e., indirect damage) by evaluating the components’ operational state $is_m = \{0, 1\}$, on the basis of the following rule:
 - 1.5.4.1 if the V_m voltage value of the m -th node is beyond the allowable limits AL (i.e., upper and lower acceptable voltage values), $V_m \notin AL$, the m -th component fails due to the cascading effects and its operational state is set $is_m = 1$;
 - 1.5.4.2 if $V_m \in AL$, the m -th node withstands the cascading effects and $is_m = 0$, for each operative component is attributed.
 - 1.5.5 Results are collected in the “indirect damage” matrix $\bar{\bar{I}} D = (\bar{\bar{C}}, \bar{\bar{IS}})$, whose m -th row is $\bar{IS}_m(is, w)$, where the vector \bar{IS} summarizes the is_m operational states of the m -th components and the amount of power not supplied w_m by the m -th failed nodes due to the indirect damage, that, in practice is the power demand PD that should have been supplied by those nodes.
 - 1.5.6 The $\bar{\bar{S}} E$ matrix is used to evaluate the disruption of the socio-economic activities that depend on power supply due to power outage (i.e., systemic damage), in terms of number u and typology b of affected customers: for each m -th node not supplying w , the number and category of connected customers, is calculated.
 - 1.5.7 Results are collected in the “systemic damage” matrix $\bar{\bar{S}} D$, whose b -th row is $\bar{SD}_b(u)$, where the scalar u summarizes the number of affected customers for each b -th category due to the systemic damage.

1.5.8 $j = j + 1$ and return to 1.5.1.

2 Indicators evaluation:

2.1 For the k -th component type, the expected Number of Failed Components (NFC) is calculated as the total number of m -th components that results in direct operational state $ds_m = 1$ (i.e., failed) due to the direct damage, and expressed as in Eq. (1):

$$NFC_k = \sum \text{number of components with } (ds_m = 1) \quad (1)$$

2.2 For the b -th customer category, the expected Power Not Supplied (PNS) is computed as the total amount of power not supplied w_m by the m -th components resulting in indirect operational state $is_m = 1$ (i.e., failed) due to the indirect damage, and expressed as in Eq. (2):

$$PNS_b = \sum \text{power demand of components with } (is_m = 1) \quad (2)$$

2.3 For the b -th customer category, the expected Number of Affected Customers (NAC) is given by the total number of connected customers to the sum, $\sum m$, of the m -th nodes not supplying $w_m > 0$, and expressed as in Eq. (3):

$$NAC_b = \sum \text{number of customers connected to nodes with } (w_m > 0) \quad (3)$$

3. $i = i + 1$ and return to 1.1.

By repeating the whole process for I hazard scenarios of different years of return period T , the framework can enable finding the most critical components for the security of power supply during flooding events and its outcomes can assist stakeholders, public authorities and policy makers to formulate effective risk mitigation strategies for guaranteeing public security and ensuring financial well-being.

2.2. Models

In the case study, the framework is applied, without loss of generality, relying on models selected from the literature, adequate to the type of available data and capable to leanly feed one model with the outputs of the other.

2.2.1. Flood inundation modeling

The flood is simulated by solving the shallow water equations, which are a version of the Navier-Stokes equations to describe the motion of fluids in three dimensions [32]. We use the consolidated two-dimensional (2D) hydraulic model implemented in the HEC-RAS software [33]. The modeling capabilities of HEC-RAS on two dimensions have been tested through a benchmark analysis, which has proved that it performs extremely well compared to other 2D models [34].

This study focuses on fluvial flooding and does not consider pluvial flooding or the combination of the two (i.e., compound events). The runoff conditions of the stormwater drainage system are not considered because this would require coupling the 2D hydraulic model with a one-dimensional (1D) model to represent both the pipe network and floodplain area (i.e., 1D/2D hydraulic models), which, however, requires more data, increases the simulation time and introduces instability issues over the 1D/2D boundaries. For the purpose of this study, the inclusion of drainage in the hydraulic model of the synthetic case study would add no further value, but it should be considered for the assessment of a real case.

2.2.2. Network modeling

In absence of real data, the network is modeled synthetically by adapting the IEEE 14 power grid benchmark [31]. More details are supplied in Section 3.1.

2.2.3. Fragility analysis

Fragility curves have been defined based on the technical data sheets of the Italian power grid ([35]; e-distribuzione S.p.A., 2024b) to describe the relationship between the hazard intensity variable and the probability of damage to network components. To the authors' knowledge, this is the first time that fragility curves are defined for a large number of different components of a power grid [36,37], since the fragility curves are usually available only for substations as a function of the accumulated rainfall [14], and are hard to apply in contexts different from the one in which they have been calibrated (FEMA, 2022). Here, the fragility of the m -th component is defined as the probability of its failure, denoted as $p_{f,m}$, when the inundation height at the component location $h_{w,m}(x,y)$ exceeds the m -th component height $h_{e,m}(x,y)$:

$$p_{f,m} = P[h_{w,m} > h_{e,m}] \quad (4)$$

Different causes of failure of the high voltage (HV) substations and medium voltage (MV) secondary cabinets can be induced by flooding (Fig. 2). For substations, the generic height is taken as $h_e = 0.2$ m: above this height, floodwater enters from the air vents in the prefabricated metal kiosks, causing damage to the peripheral protection, command and control systems housed therein, with $p_f = 1$

if inundation height $h_w > 3$ m for which floodwater comes into physical contact with the electrical conductors and insulators mounted at ground level in the switchyard [35]; for $0.2 < h_w < 3$ m, p_f follows the continuous (with stars) line of Fig. 3. For the secondary cabins, instead, $h_e = 0.18$ m with a maximum height equal to 0.4 m: if the floodwater enters the secondary cabin through the air vents, it comes into physical contact with the internal electrical equipment, leading the cabin to fail (e-distribuzione S.p.A., 2024b); for $0.18 < h_w < 0.4$ m the fragility curve follows the continuous (with triangles) line of Fig. 3. The failure probability of the (HV) substations and (MV) secondary cabins is simulated by direct Monte Carlo simulation [38] meaning that, for each h_w originated by the i -th flooding scenario, $i = 1, 2, \dots, I$, we sample J random numbers r_j from the uniform distribution $U(0, 1)$: if the failure probability $p_{f,m}|h_w$ of the m -th component when exposed to a floodwater level h_w exceeds r_j , the m -th component fails, otherwise not (Eq. (5)). In other words, at each j -th iteration, we assume binary states $ds_m = \{0, 1\}$ for each m -th power grid component: either fully operative (0) or totally failed (1).

$$ds_{m,j} = \begin{cases} 1 & \text{if } p_{f,m}(h_w) > r_j \\ 0 & \text{if } p_{f,m}(h_w) < r_j \end{cases} \quad (5)$$

Direct damages to steel lattice towers [39] and concrete poles [40,41], as well as damages to underground cables are not considered due to lack of adequate tools (i.e., soil erosion models) that provide estimates of the erosion phenomena they are exposed to (e.g., scour depth); overhead lines are not considered vulnerable to flooding, and power plants and synchronous condensers are outside the scope of this study.

2.2.4. Power flow modeling

The power flow is simulated using MATLAB Simulink software [42], a widely used scientific tool to analyze the performance of a network in steady-state operation. Its computational algorithm relies on the Newton-Raphson iterative method, which solves the nonlinear system of power flow equations, providing a robust and fast convergence solution. The required inputs are the line (i.e., edge) conductance $G_{m,\delta}$ (reciprocal of the R resistance) and susceptance $B_{m,\delta}$ (reciprocal of the X reactance) between the m_γ and m_δ components of the power grid.

Power flow models calculate the voltage magnitude V_m and phase angle θ_m at each m -th component, for specified net active power P_m , reactive power Q_m and voltage conditions, respectively:

$$P_m = PG_m - PD_m \quad (6)$$

$$Q_m = QG_m - QD_m \quad (7)$$

in which PG_m is the active power and QG_m is the reactive power of each m -th component that supplies power to the grid, whereas PD_m is the active power and QD_m is the reactive power that flows to each m -th component that demand power from the grid.

The comparison of P_m and Q_m with the network allowable limits allows identifying the portion of the network (i.e., the number and

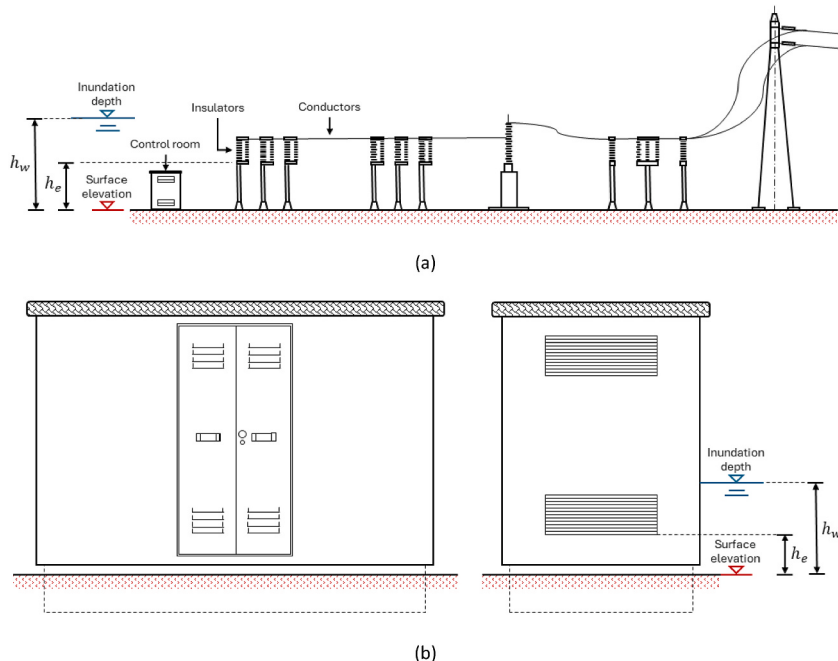


Fig. 2. Schematics of the inundation scenarios of (a) substations and (b) secondary cabins.

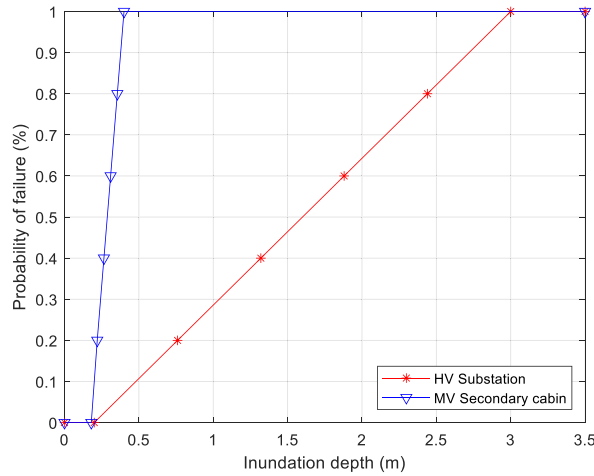


Fig. 3. Fragility curves of high voltage (HV) substations and medium voltage (MV) secondary cabins.

the location of the electrical HV substations and MV secondary cabins) that goes out of service. This is measured by the \bar{V} voltage profiles of the \bar{C}_m power grid components: when the voltage V is below or above the allowable limits, the m -th component is not able to supply power to the connected customers. By so doing, we evaluate to what extent power supply is secured and the exposure of the network to flooding.

2.2.5. Service area analysis

Service areas have been modeled by referring to real data on power consumption in Italy. More details are supplied in Section 3.1.3.

3. Case study

The proposed framework has been applied to a synthetic case study concerning a power supply network, whose spatial characterization, hazard features, components fragility, economic and societal area information are provided in Section 3.1, as well as assumptions made to cope with data collection difficulties expected in practice.

3.1. Model set-up

The synthetic case study is adapted from the IEEE 14 power grid benchmark [31]. The characteristics of the synthetic environment have been defined to represent reality as closely as possible, in terms of the flood hazard, the power grid features, and the supplied socio-economic activities. In particular, a spatial dimension has been allocated to the benchmark. This means also that the power losses due to the resistance of the lines and the cables to the power transmission over long distances is to be estimated and duly accounted: to consider this, the technical specifications of the electrical conductors based on the technical standards of the Italian power grid for both the HV and MV levels are assumed and listed in Table 1 ([35]; e-distribuzione S.p.A., 2024b).

Although the IEEE 14 power grid refers to a transmission benchmark, a distribution network is built by converting the HV to MV with the use of transformers. The integration of all three levels of power grid (i.e., generation, transmission and distribution) requires an analysis at the meso-scale. For this reason, we assume that the benchmark mimics the positioning of numerous realistic power grid components at a provincial level (for a spatial size of approximately equal to 2500 km^2), considering its power generation and demand values. These components include overhead lines and underground cables, electrical substations and cabins, power plants and synchronous condensers; moreover, steel lattice towers and concrete poles that were missing in the benchmark have been added.

A conceptual representation of the area of interest is sketched in Fig. 4, while the effective spatial distribution is shown after, in Fig. 5. $Z = 14$ service areas are modeled, with different social and economic characteristics, classified in such a way to consider the different type of customers connected: $\bar{SE}_m = 10, 12, 14$, are three small towns, whose residents depend on the $\bar{SE}_m = 6, 9, 13$

Table 1

The resistance, reactance, inductance and capacitance parameters of lines and cables in the transmission and distribution network.

Parameters	Transmission		Distribution	
	Lines	Cables	Lines	Cables
Resistance (Ω/km)	0.05674	0.02230	0.23025	0.16435
Reactance (Ω/km)	0.38327	0.07226	0.35500	0.17907
Inductance (H/km)	0.00122	0.00023	0.00113	0.00057
Capacitance (F/km)	9.48E-09	8.11E-08	1.03E-08	2.20E-08

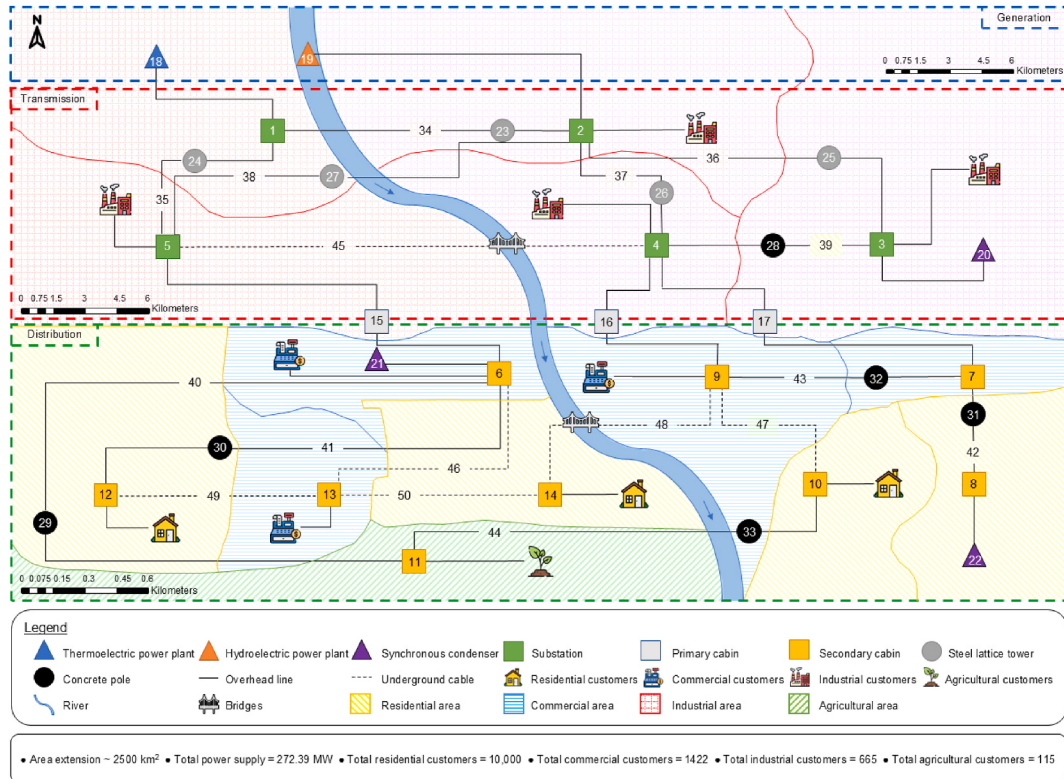


Fig. 4. Sketch of the conceptual representation of the area of interest, crossed by the river (i.e., the hazard source), the power grid systems and components (i.e., generation, transmission and distribution) and the services areas; yellow polygons represent the residential areas, blue the commercial, red the industrial and green the agricultural.

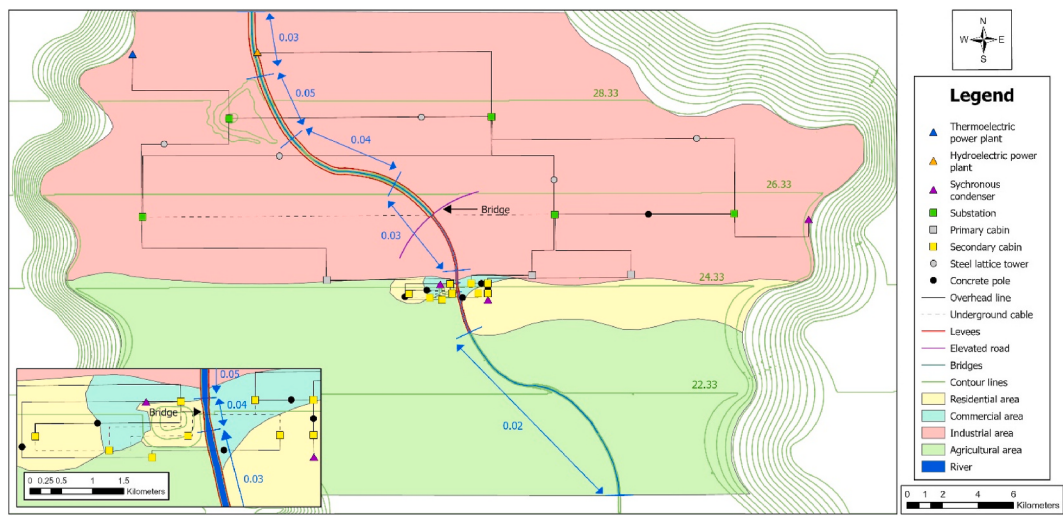


Fig. 5. Effective spatial distribution of the area of interest; contour lines of 2 m intervals, land use areas in the floodplain, land cover cross-sections for the river channel, levees, bridges, and an elevated road.

commercial areas, the $\overline{SE}_m = 2, 3, 4, 5$ industrial facilities, that are power supplied directly by the transmission network, and the \overline{SE}_{11} agricultural area. Three service areas $\overline{SE}_m = 1, 7, 8$, do not supply power to customers. The separation between service areas, particularly between residential and commercial, is a simplification.

Power is generated by the thermal power C_{18} and the hydroelectric power C_{19} plant, which are connected to the substations C_1 and

$\overline{C_2}$, respectively. The transmission network has a nominal voltage of 132 kV, whereas the distribution network of 20 kV. The transmission network is composed of $\overline{C_m} = 1, \dots, 5$ that are switching substations, and $\overline{C_m} = 6, \dots, 14$ that are secondary switching cabinets that shape the distribution network. Three primary transformer cabins, $\overline{C_m} = 15, 16, 17$, link the transmission network to the distribution network. Three synchronous condensers, $\overline{C_m} = 20, 21, 22$, one in the transmission network and two in the distribution network, adjust the voltage fluctuations.

Both the distribution and the transmission networks are assumed to be linked by overhead lines, $\overline{C_m} = 34, \dots, 44$, and underground cables, $\overline{C_m} = 45, \dots, 50$, in a proportion that mimics the characteristics of the Italian power grid: 1 out of 7 (approximately 14 %) connections between the switching substations are made of underground cables whereas between secondary switching cabinets that percentage reaches 50 % [43]. Besides, the transmission network is mainly composed of steel lattice towers, $\overline{C_m} = 23, \dots, 27$, except of one $\overline{C_{28}}$ concrete pole, whereas the distribution network is explicitly made of concrete poles, $\overline{C_m} = 29, \dots, 33$. A shunt capacitor bank is connected to the secondary cabin $\overline{C_9}$ to reduce the system power losses, provide voltage control, and increase the system capacity. Other voltage control devices/systems (e.g., automatic voltage regulators, static generators, power inverters) that can provide fast-response reactive power compensation in case of voltage violation are not considered. Network components characteristics are summarized in Table 2, along with the vulnerability parameters that influence their physical damage, and their probability of failure.

In Table 3, an extract of the \overline{C} matrix is shown. The complete matrix is available in Appendix A.

The region is crossed by a river, whose geometric and hydraulic features are discussed in Section 3.1.1, along which power plants and service areas are located; the other components are spatially distributed according to the average distance values in the Italian territory ([44]; e-distribuzione S.p.A., 2024a).

3.1.1. Flood

The framework is applied, without loss of generality, to the selected hazard scenarios with return time T_{20} , T_{50} , T_{100} , T_{200} , and T_{500} (each scenario is associated with an occurrence probability). Flood inundation modeling is composed of data pre-processing, hydraulic modeling and data post-processing. In pre-processing, the generation of river channel bathymetry and floodplain area is carried out. This has been done in ArcGIS PRO software, by spatially locating the position of stream centerline, riverbanks, levees (that protect adjacent areas from flooding), bridges (piers obstruct the water flow), and an elevated road for the creation of a DTM (see Fig. 11 of Appendix A), here assumed with a resolution of 5 m (that has been considered as sufficient for the accurate representation of the area in terms of capturing surface irregularities and for numerical purposes). Without loss of generality, we assume that this results in a rectangular river channel of 5 m deep and 120 m width, with additional contractions and expansions nearby the bridges. The floodplain area results in a flat valley located between two high hills, where the meandering river flows slowly towards the lower elevation.

The hydraulic modeling requires as inputs the terrain layer, the n Manning's roughness coefficients, the boundary conditions, the geometric data and the turbulent mixing. The terrain layer is based on the abovementioned DTM; the n Manning's roughness coefficients are derived by the classification of land cover and land use: land cover indicates the physical type of land (e.g., crops, grass, water, built-up area, etc.), while land use means the socio-economic use of land (e.g., agriculture, forestry, recreation, residential use, etc.). In detail, the land cover/use layer of the investigated area is classified into eight district regions (each one assigned with different n Manning's roughness coefficient): four within the river channel, $n_{high} = 0.05$, $n_{medium} = 0.04$, $n_{low} = 0.03$ and $n_{verylow} = 0.02$, to represent vegetation densities, and four in the floodplain area, $n_{res} = 0.06$, $n_{com} = 0.06$, $n_{ind} = 0.06$ and $n_{agr} = 0.04$, to determine areas occupied by the different socio-economic activities, as shown in Fig. 5. The classification of land use in the area of interest is coherent with the classification of the service areas.

Two different types of boundary conditions have been used: a hydrograph and a normal depth. The hydrograph boundary condition is located upstream, at the starting point of the river, representing the flow rate (i.e., discharge) entering the river within the time

Table 2
Parameters to be considered for the assessment of component physical vulnerability.

k^{th} type	λ^{th} system	m^{th} component	Vulnerability parameters
Overhead lines	Transmission	$\overline{C_m} = 34, \dots, 39$	Installation depth, carrying capacity
	Distribution	$\overline{C_m} = 40, \dots, 44$	
Underground cables	Transmission	$\overline{C_{45}}$	
	Distribution	$\overline{C_m} = 46, \dots, 50$	
Steel lattice towers	Transmission	$\overline{C_m} = 23, \dots, 27$	Installation depth, carrying capacity
	Transmission	$\overline{C_{28}}$	
Concrete poles	Distribution	$\overline{C_m} = 29, \dots, 33$	
	Transmission	$\overline{C_m} = 1, \dots, 5$	
Substations	Transmission	$\overline{C_m} = 15, 16, 17$	Electrical equipment elevation, pumping
Primary cabins	Distribution	$\overline{C_m} = 6, \dots, 14$	equipment installation, flood barrier
Secondary cabins	Distribution	$\overline{C_{18}}$	system, air vents height, voltage level
Thermal power plant	Generation	$\overline{C_{19}}$	Equipment installation height, flood
Hydroelectric power plant	Generation	$\overline{C_{20}}$	barrier system, nominal capacity
Synchronous condensers	Transmission	$\overline{C_m} = 21, 22$	
	Distribution		

Table 3

Network components characteristics ($\bar{\bar{C}}$) (the complete Table is reported in Appendix A).

$\bar{\bar{C}}$	x cartesian coordinate	y cartesian coordinate	k type of component	λ system of power grid
x_1		y_1	substation	transmission
x_2		y_2	substation	transmission
x_3		y_3	substation	transmission
:		:	:	:
x_{50}		y_{50}	underground cable	distribution

during a flooding scenario $Q_{T,in}(t)$. Fig. 6 shows the hydrographs for the considered floods with T_{20} , T_{50} , T_{100} , T_{200} , and T_{500} . To fulfill the purpose of this research, hydrographs are synthetically developed by the authors, without a prior hydrological analysis, using the Adda as a reference river given that its features (e.g., size, watershed) are similar to those assumed here [45]. The second boundary condition is defined downstream, in the ending point of the river, in terms of a discharge-water depth relation corresponding to a normal depth. Normal depth assumes uniform flow conditions by imposing the friction slope to equal the bed slope of the river channel.

The model calculates the water surface at each computation cell of the mesh at each time step. In this study, a computational mesh of 5 m within the river channel and 50 m in the floodplain area is selected. Computational time intervals are equal to 2 s. The total length of the simulated stream reach is approximately 37 km. The approach of eddy viscosity v_t has been used to include the effects of turbulence in the 2D flow area.

Post-processing consists in graphically representing the outputs of the 2D hydraulic model, here done in ArcGIS PRO environment: the focus is on sketching the h_w water depth values estimated by the 2D hydraulic model in correspondence of the M power grid components.

3.1.2. Power network

In Table 4, an extraction of the matrix $\bar{\bar{P}}$ is shown (the complete matrix is available in Appendix A), where the active PG and reactive QG power generation, the active PD and reactive QD power demand, the physical parameters (i.e., the length L , resistance R , and reactance X), of each \bar{C}_m component of the power grid, has been listed, equal to the typical values of the benchmark.

Fig. 7 compares the network performance of the IEEE 14 power grid benchmark and the synthetic case study (i.e., considering the modifications made to take into account the spatial dimension) under nominal conditions (i.e., no flood), by examining their overall voltage profiles. We observe that the voltage profile in the case study differs from that of the benchmark, specifically after the voltage drop for the transition from the transmission to the distribution system, due to the lengthening or shortening of the lines and cables connecting the relative cabins, without, however, derailing the V_m voltage magnitude outside the allowable limits (here considered equal to $\pm 5\%$ of the nominal values), making the case study enough realistic and suitable for the purpose of the present work.

3.1.3. Service areas

The power demand values considered are those publicly available at the regional level in Italy and supplied by Terna, the single operator managing the Italian transmission grid [44]; in this work, the Lombardy region is used as reference area and power demand values for the year 2021 are considered. The total number of customers is taken from the data provided by the national institute of

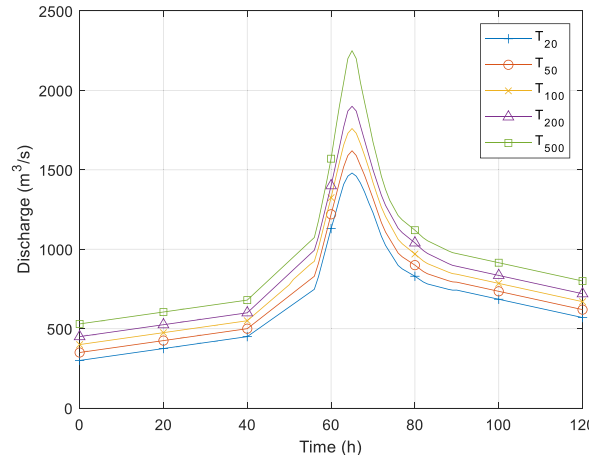


Fig. 6. Hydrographs for the scenarios of T_{20} , T_{50} , T_{100} , T_{200} , and T_{500} .

Table 4

The active and reactive power generation, the active and reactive power demand, and the physical parameters (i.e., the length, resistance, and reactance), of each power grid component (matrix \bar{P}).

\bar{P}						
Active power generation (MW)	Reactive power generation (MVar)	Active power demand (MW)	Reactive power demand (MVar)	Length (km)	Resistance (Ω)	Reactance (Ω)
0	0	0	0	0	0	0
21.7	12.7	0	0	0	0	0
94.2	19.0	0	0	0	0	0
:	:	:	:	:	:	:
0	0	0	0	0.625	0.103	0.102

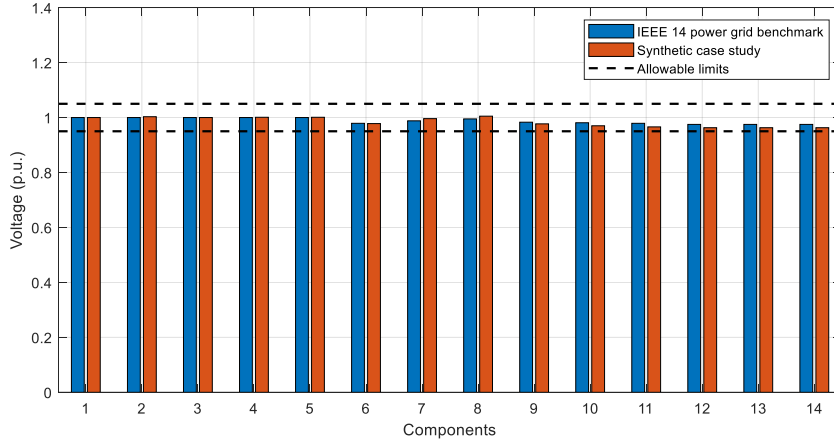


Fig. 7. Voltage magnitudes of the components for the nominal condition of the IEEE 14 power grid benchmark, for the nominal condition in the synthetic case study, and the allowable limits.

statistics (ISTAT) for the year 2011, assuming that all socio-economic activities are connected to the power grid. The average consumptions per year of the various categories is estimated, to proportionally allocate to each the corresponding share of PD active power demand values, as shown in $\bar{S} E$, whose extract is in [Table 5](#) (the complete matrix is available in Appendix A), characterizing the total number a of b type of customers connected to each C_m electrical substation and cabin of the power grid.

Table 5

Extract of the socio-economic matrix $\bar{S} E$ characterizing the number and category of customers connected to each power grid component; customers are connected only to substations and secondary cabins.

$\bar{S} E$	
a number of customers	b category of customers
0	industrial
47	industrial
204	industrial
104	industrial
16	industrial
294	commercial
0	commercial
0	residential
774	residential
3000	residential
115	agricultural
2033	residential
354	commercial
4967	residential
0	no customer category connected
:	:
0	no customer category connected

4. Results

The results of the 2D hydraulic modeling are summarized in Fig. 8, whereas the result of their overlapping with the topological model is given in Table 6, where the exposure matrix \bar{E} of the components of the power grid exposed to flood risk is reported. In the hazard scenario T_{20} , when the hydrograph is getting closer to the peak, the river starts overtopping the levees that protect the distribution network from flooding. The overflow starts before the contraction of the river due to the presence of a bridge that connects two residential service areas. Most flood water overflows to the right bank of the river, but within a certain time the left bank is getting also inundated; as a consequence, the distribution network is inundated. In detail, the $C_m = 6, 7, 8, 9, 10, 11, 12, 13$ secondary cabins are flooded. In the hazard scenarios T_{50} , T_{100} and T_{200} , the flooding mechanism does not change but, as expected, the inundation depth values at cabins, as well as the total inundation area, increase in line with the increase of flooding discharge. It is worth pointing out that the only cabin of the distribution network that remains untouched by the flood wave in all the scenarios is the \bar{C}_{14} secondary cabin, which is located in a hilly area. During the most intense hazard scenario T_{500} , the transmission network is also inundated by high water depth values, due to the overflowing of 3 m high levee that protect it, leading to the flooding of \bar{C}_1 substation.

4.1. Direct damage

Fig. 9 elaborates the information extracted from the simulations and stored in direct damage matrix $\bar{\bar{D}}$, as reported in Appendix A, and shows the number of components that fail because of inundation, for the different hazard scenarios considered and for the $J = 100$ different components failure scenarios generated. We notice that for the hazard scenario T_{20} the number of failed secondary cabins range from 1 to 4, with the value of 2 having the highest probability density. In the hazard scenario T_{50} , the range of possible values increases, varying between 2 and 6, with the highest probability density for the value 4. In the hazard scenario T_{100} , 6 secondary cabins are more likely to fail. For the hazard scenario T_{200} , the number of secondary cabins with the highest probability to fail is 7. Finally, for the catastrophic hazard scenario T_{500} , it is likely that all secondary cabins of the distribution network turn out to fail except for \bar{C}_{14} , whereas the transmission network is likely affected by the failure of the \bar{C}_1 substation. The effects of the failure of \bar{C}_1 , which is the closest to the \bar{C}_{18} , brings severe consequences on $\bar{\bar{D}}$, meaning that \bar{C}_1 is a critical asset, as we shall see in what follows.

4.2. Indirect damage

Fig. 10 shows the performance of the transmission and distribution networks, measured by the unsupplied power from grid components, as determined through power flow modeling. In the hazard scenario T_{20} , the failure of secondary cabins due to inundation causes the disruption of other secondary cabins, that are not exposed to flooding, due to cascading effects in the distribution network. For this reason, the power grid does not supply power to residential, commercial, and probably agricultural customers, with the total amount of power not supplied w to them of the highest probability density being 6.1 MW out of 30 MW (20 %) for the residences, 24.7 MW out of 54.2 MW (46 %) for the businesses, and all 3.5 MW (100 %) for the agricultures, respectively. Paradoxically, in the hazard scenario T_{50} of greater magnitude, more secondary cabins probably fail because of the direct damage, but less secondary cabins may completely fail at the end. In particular, \bar{C}_{14} secondary cabin, that supply power to a residential service area, can remain fully operative: this is explained by the fact that the overall power demand is reduced as a consequence of the failure of several secondary

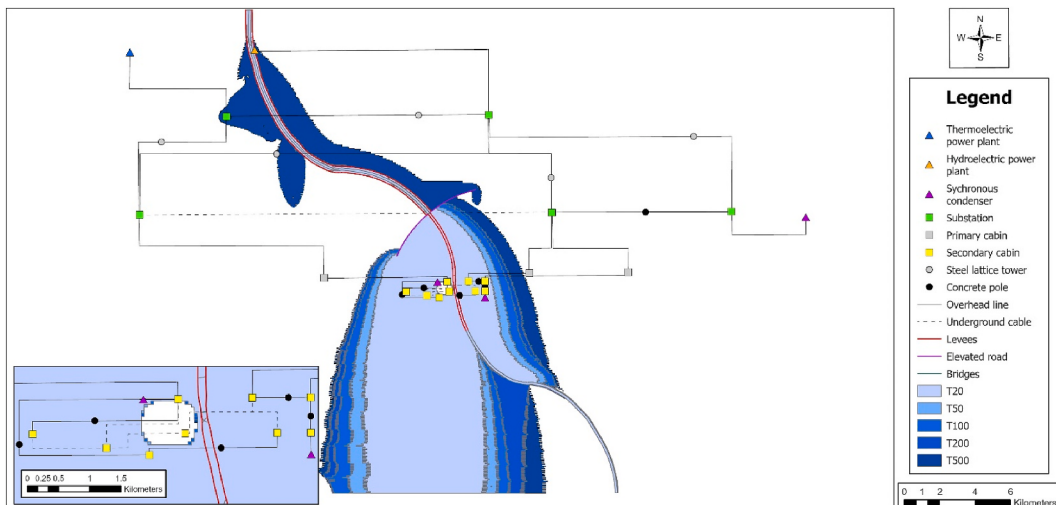


Fig. 8. Hazard map for floods of different return periods.

Table 6Power grid components exposed to floods of different frequency (matrix $\bar{\bar{E}}$).

$\bar{\bar{E}}_{T_{20}}$	$\bar{\bar{E}}_{T_{50}}$	$\bar{\bar{E}}_{T_{100}}$	$\bar{\bar{E}}_{T_{200}}$	$\bar{\bar{E}}_{T_{500}}$
Exposed component	Exposed component	Exposed component	Exposed component	Exposed component
$\overline{C_6}$	$\overline{C_6}$	$\overline{C_6}$	$\overline{C_6}$	$\overline{C_1}$
$\overline{C_7}$	$\overline{C_7}$	$\overline{C_7}$	$\overline{C_7}$	$\overline{C_6}$
$\overline{C_8}$	$\overline{C_8}$	$\overline{C_8}$	$\overline{C_8}$	$\overline{C_7}$
$\overline{C_9}$	$\overline{C_9}$	$\overline{C_9}$	$\overline{C_9}$	$\overline{C_8}$
$\overline{C_{10}}$	$\overline{C_{10}}$	$\overline{C_{10}}$	$\overline{C_{10}}$	$\overline{C_9}$
$\overline{C_{11}}$	$\overline{C_{11}}$	$\overline{C_{11}}$	$\overline{C_{11}}$	$\overline{C_{10}}$
$\overline{C_{12}}$	$\overline{C_{12}}$	$\overline{C_{12}}$	$\overline{C_{12}}$	$\overline{C_{11}}$
$\overline{C_{13}}$	$\overline{C_{13}}$	$\overline{C_{13}}$	$\overline{C_{13}}$	$\overline{C_{12}}$
				$\overline{C_{13}}$

cabins and the grid has managed to adapt to the new conditions due to its dynamic complexity (i.e., the characteristic of continuous adaptation to new power demand conditions) and the arising cascading effects. Nevertheless, the amount of power not supplied to domestic customers with the highest probability density increases up to all 30 MW (100 %).

In the scenario T_{100} , the increased number of failed secondary cabins more probably causes the disruption of power supply to the entire distribution network, except for $\overline{C_7}$ and $\overline{C_8}$ secondary cabins (on which no socio-economic activities are power-dependent), thus resulting in an amount of power not supplied to commercial customers equal to all 54.2 MW (100 %). However, for the hazard scenario T_{200} , as expected for a scenario of larger magnitude, this probability becomes equal to 1. Finally, for the catastrophic hazard scenario T_{500} , the entire power grid is likely to collapse due to the failure of $\overline{C_1}$ substation that, as already said, is a critical asset. Indeed, such substation plays a key role in securing power supply, especially to industries, whose power interruption amounts to 171.3 MW (100 %), that is equal to the whole amount needed by the other three categories. Results of the analysis are also included in the indirect damage matrix $\bar{\bar{I}} D$, as reported in Appendix A.

4.3. Systemic damage

In Fig. 10, the socio-economic impact, in terms of power outage impact on customers, is illustrated, as obtained by the service area analysis. The impact is measured by the u number of customers of the b customer categories affected by the power interruption at steady state. For the hazard scenario T_{20} , residential, commercial, and probably agricultural activities face power interruption problems. More specifically, 2000 out of 10,000 (20 %) residential customers, 648 out of 1422 (46 %) commercial customers and all the 115 (100 %) agricultural customers most probably remain without electricity. In line with the results of power flow analysis, the hazard scenario T_{50} can be less catastrophic in terms of socio-economic impact, as less residential activities may be affected. Despite, the number of affected residential customers with the highest probability density increases up to all 10,000 (100 %). The hazard scenarios T_{100} and T_{200} , show an increase in the number of commercial customers affected, all 1422 (100 %), as expected. However, it is important to point out that more probably the socio-economic impact of these two hazard scenarios is similar, even if the magnitude of the events is different. The direct damage for scenario T_{100} shows that MV secondary cabins failure is likely to damage the entire distribution network, except for those not serving socio-economic activities. Thus, even when more failures occur, i.e., scenario T_{200} , the socio-economic impact does not change. Finally, in the catastrophic hazard scenario T_{500} , all customers connected to the power grid are more probably affected, including industrial activities, thus resulting in a great w amount of power not supplied, as previously mentioned, although the u number of affected industrial activities is significantly low. Results of the analysis are also reported in the systemic damage matrix $\bar{\bar{S}} D$, as reported in Appendix A. Results show that damages to power-dependent socio-economic activities extend far beyond the initial inundation area due to the cascading failures within the interconnected power grid.

5. Discussion

Existing methodologies for the assessment of flood risk to power grids are, to some extent, incomplete, as they typically focus on specific types of damage only, while oversimplifying or overlooking others. A comprehensive framework is instead needed to: (i) estimate flood damages to the power grid components, (ii) analyze cascading failures in the network, and (iii) assess the impact of power outages on customers. In this paper, we have proposed a probabilistic modeling and simulation framework integrating various modeling techniques for the comprehensive assessment of flood risk to power grids by systematically accounting for the full spectrum of expected damages.

The results of the application of the framework can allow decision-makers to evaluate the effectiveness of risk mitigation measures, both structural (e.g., increasing the height of electrical equipment contained in the substations, increasing the elevation of the ventilation holes of cabins) and non-structural (e.g., implementation of real-time dispatch strategies), to secure power supply during flooding events [46–48]. A cost-benefit analysis could, then, be performed using, for example, multi-criteria optimization with twofold benefits. On the one hand, from the perspective of grid operators, the identification of the optimal mitigation measures to be

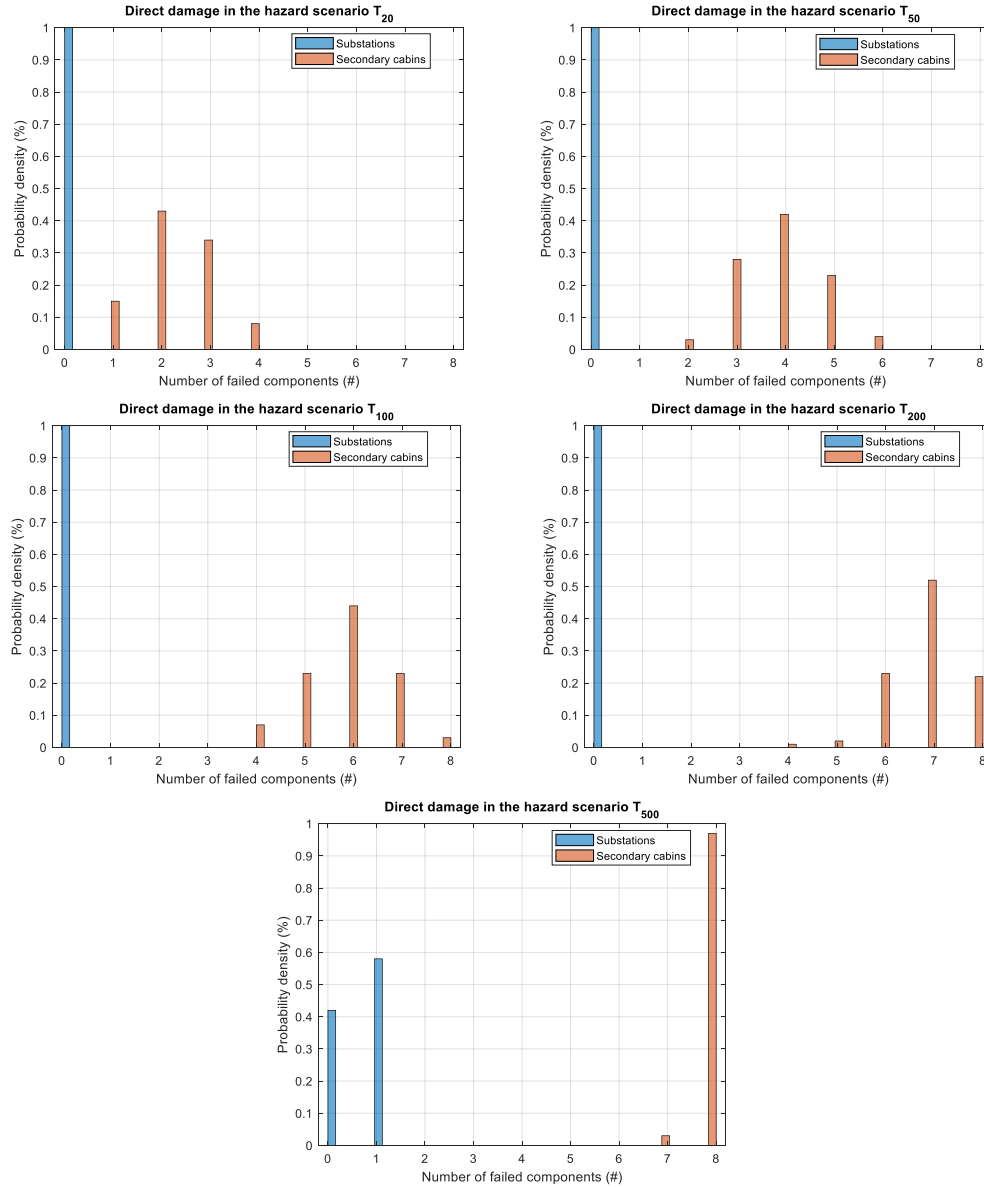


Fig. 9. Probability density of the number of power grid components failed due to inundation for each component type for floods of different frequency; operational state is evaluated only for substations and secondary cabins.

implemented would reduce the economic losses caused by not supplying customers; on the other hand, from the perspective of civil protection authorities, the secured functioning of the power grid would contribute to the effective emergency management in case of flood (e.g., power supply to hospitals, transportation, etc.).

The proposed framework relies on empirical data regarding damage mechanisms, which are difficult to obtain for two reasons: on the one hand, they pertain to different systems (generation, transmission and distribution) spanning multiple territories and jurisdictions; on the other hand, they are often deemed sensitive as they relate to national CIs [49]. Yet the applicability, strength and benefit of the framework has been shown under the assumptions summarized in Table 7.

Future efforts will focus on validating the framework using real data. This can be facilitated by enforcing an extensive post-flood data collection activity in collaboration with grid operators, in particular for the characterization of the components' fragility curves. Engaging civil protection agencies can, instead, provide valuable insights to more realistically model the socio-economic impacts of flooding on electricity-dependent sectors. The ultimate objective is the development of a resilience-based probabilistic modeling and simulation framework to inform mitigation strategy decision-making. This will encompass not only the effects of disruption caused by flooding, but also the alternatives offered by post-disruption recovery strategies.

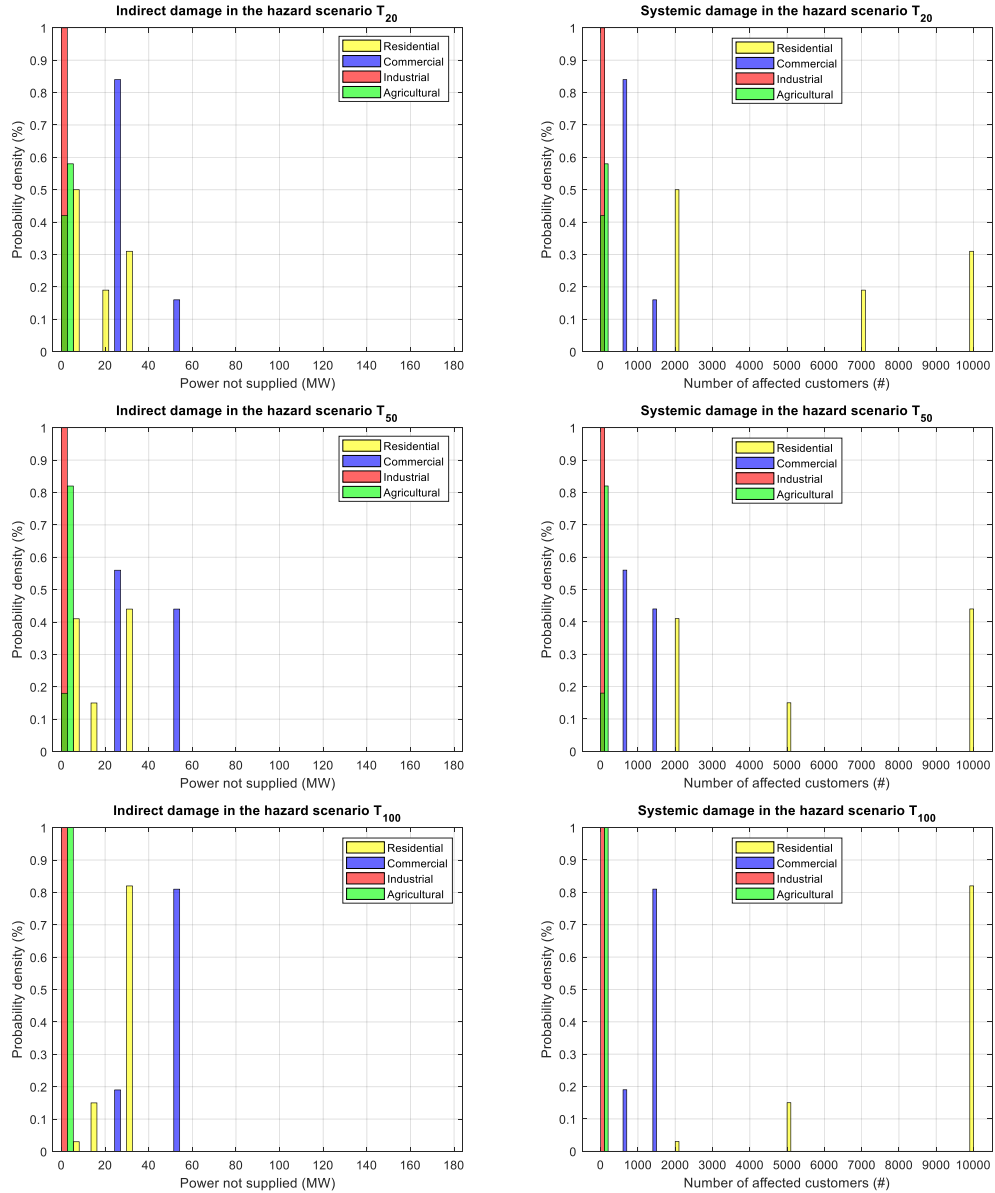


Fig. 10. Probability density of (a) the amount of power not supplied to customers due to power outage and (b) the number of customers affected by power interruption for each customer category at steady state for floods of different frequency.

6. Conclusions

In this paper, we propose a probabilistic modeling and simulation framework for the assessment of the risk to power grids due to flooding. The framework is made up of a suite of models (easily transferable to various geographic and socio-economic contexts) for

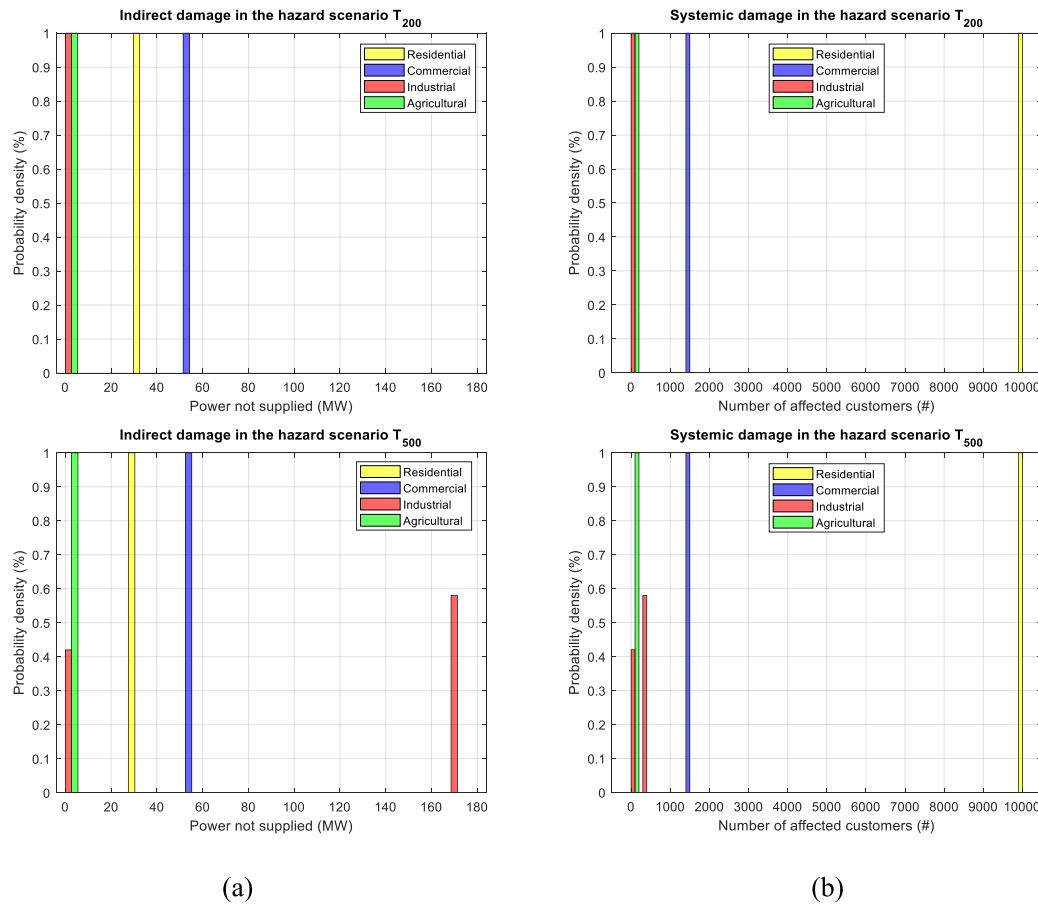


Fig. 10. (continued).

Table 7
Overview of assumptions.

	Assumptions
Models	Hydrographs are synthetically developed, drawing inspiration from a similar river. The power grid components are removed from the network in case of failure. Each component serves only one customer category. The total number of customers served is estimated assuming that all the activities connected to the power grid are running at the maximum power.
Physical system	The benchmark mimics the spatial positioning of realistic components at a provincial level, in Italy. The meandering river bathymetry results in a rectangular shape, contracting or expanding near bridges. The geometry of floodplain features a flat valley between two hills. The geometry of hydraulic structures (e.g., levees, bridges) is synthetically generated for the specific case. The DTM resolution is empirically selected to accurately represent the area. The Manning's roughness coefficients are derived from the classification of land cover and land use areas. The parameters of lines and cables are determined based on the standard technical specifications.

identifying the components of the power grid that fail when exposed to a flood, and evaluating the overall network performance and the power outage impact on the customers in terms of direct (i.e., failure of components), indirect (i.e., loss of network functionality) and systemic (i.e., disruption of socio-economic activities) damages; these are measured by the number of components failed due to

inundation for the different component types, the amount of power not supplied to the different customer categories at steady state conditions, and the number of customers affected by the power interruption for the different customer categories, respectively. The most critical components of the network (whose failure affects most customers and results in largest power supply disruption) can be identified.

The approach has been exemplified by means of a synthetic case study, which is based on the IEEE 14 power grid benchmark. In particular, we have used a stochastic generator of hazard scenarios of different probabilities of occurrence, fragility curves of electrical substations and cabins to determine their failure probability when exposed to the hazard, power flow distributed model to quantify the voltage profile of the network following the disruption, and finally a socio-economic model to assess the impacts of power outages on the connected residential, commercial, industrial and agricultural customers. Results show that damage to power-dependent socio-economic activities is likely to propagate far from the inundation area. This is due to the fact that the failure of certain components may initiate a sequence of cascading effects and failures in the power grid, which arise as a consequence of its interconnected nature. These effects must be taken into consideration when designing the mitigation measures to counteract the flooding escalation and the power curtailment.

The probabilistic modeling and simulation framework enables decision-makers to conduct thorough and consistent risk assessments, effectively evaluating the capacity of both structural and non-structural mitigation measures to maintain power supply security during floods. Upcoming research will include the validation of the framework in real cases and the extension to a resilience-based probabilistic framework to aid decision-making in post-disruption recovery.

CRediT authorship contribution statement

Panagiotis Asaridis: Writing – review & editing, Writing – original draft, Methodology, Formal analysis, Data curation, Conceptualization, Software. **Daniela Molinari:** Writing – review & editing, Writing – original draft, Supervision, Methodology, Conceptualization, Funding acquisition. **Francesco Di Maio:** Writing – review & editing, Writing – original draft, Supervision, Methodology, Conceptualization. **Francesco Ballio:** Writing – review & editing, Conceptualization. **Enrico Zio:** Writing – review & editing, Conceptualization.

Funding

This work was supported by the PhD scholarship “Verso una valutazione esaustiva del danno a supporto della mitigazione del rischio alluvioni” funded by Banca d’Italia and developed within the PhD program in Environmental and Infrastructure Engineering at Politecnico di Milano. The participation of Francesco Di Maio to this study has been supported by the research project “Assessment of Cascading Events triggered by the Interaction of Natural Hazards and Technological Scenarios involving the release of Hazardous Substances” funded by MIUR - Italian Ministry for Scientific Research under the PRIN 2017 program (grant 2017CEYPS8).

Declaration of competing interest

The authors declare that they have no known competing financial interests or personal relationships that could have appeared to influence the work reported in this paper.

Abbreviations

CI	Critical Infrastructures
DTM	Digital Terrain Model
HV	High Voltage
IEEE	Institute of Electrical and Electronics Engineers
MC	Monte Carlo
MV	Medium Voltage
NAC	Number of Affected Customers
NFC	Number of Failed Components
PNS	Power Not Supplied
1D	One-Dimensional
2D	Two-Dimensional

List of symbols

AL	Allowable limits (i.e., upper and lower acceptable voltage values)
a	Number of customers connected to the components
B	Categories of customers
$B_{m_\gamma \delta}$	Susceptance of lines and cables between the m_γ and m_δ components
\bar{C}	Network components matrix
$\bar{D} D$	Direct damage matrix

\overline{DS}	Direct operational state vector
ds	Direct operational state (i.e., health state) of the components
\overline{E}	Exposure matrix
$FC_{k\lambda}$	Fragility curve of the k -th type of component in the λ -th system
$G_{m_\gamma m_\delta}$	Conductance of lines and cables between the m_γ and m_δ component
h_e	Equipment elevation of the components
h_w	Inundation depth
I	Number of hazard scenarios
\overline{ID}	Indirect damage matrix
\overline{IS}	Indirect operational state vector
is	Indirect operational state of the components
J	Number of components failure scenarios
K	Typologies of the components
L	Length of the components
M	Number of the power grid components
n	Manning's roughness coefficient
\overline{P}	Power matrix
P_m	Net active power flow at the m -th component
PD_m	Active power demand of the m -th component
PG_m	Active power generation of the m -th component
p_e	Annual exceedance probability of flood event
p_f	Probability of components failure due to a flood event
Q_m	Net reactive power flow at the m -th component
QD_m	Reactive power demand of the m -th component
QG_m	Reactive power generation of the m -th component
Q_T	Annual peak discharge for the return period T
$Q_T(t)$	Discharge within the t time for the return period T
R	Resistance of the components
r	Random number
\overline{SD}	Systemic damage matrix
\overline{SE}	Socio-economic matrix
s_f	Friction slope (i.e., slope of the energy grade line)
T	Return period
t	Time
u	Number of customers affected
\overline{V}	Voltage vector
V_m	Voltage magnitude of the m -th node
v_t	Eddy viscosity
w	Power not supplied to customers
X	Reactance of the components
x, y	Cartesian coordinates
Z	Number of service areas
z	Surface elevation
θ_m	Phase angle of the m -th component
Λ	Systems of the power grid
Ω	Set of Cartesian coordinates

Appendix A

Table 8Network components characteristics (matrix $\bar{\bar{C}}$).

x_1	y_1	substation	transmission
x_2	y_2	substation	transmission
x_3	y_3	substation	transmission
x_4	y_4	substation	transmission
x_5	y_5	substation	transmission
x_6	y_6	secondary cabin	distribution
x_7	y_7	secondary cabin	distribution
x_8	y_8	secondary cabin	distribution
x_9	y_9	secondary cabin	distribution
x_{10}	y_{10}	secondary cabin	distribution
x_{11}	y_{11}	secondary cabin	distribution
x_{12}	y_{12}	secondary cabin	distribution
x_{13}	y_{13}	secondary cabin	distribution
x_{14}	y_{14}	secondary cabin	distribution
x_{15}	y_{15}	primary cabin	distribution
x_{16}	y_{16}	primary cabin	distribution
x_{17}	y_{17}	primary cabin	distribution
x_{18}	y_{18}	thermal power plant	generation
x_{19}	y_{19}	hydroelectric power plant	generation
x_{20}	y_{20}	synchronous condenser	transmission
x_{21}	y_{21}	synchronous condenser	distribution
x_{22}	y_{22}	synchronous condenser	distribution
x_{23}	y_{23}	steel lattice tower	transmission
x_{24}	y_{24}	steel lattice tower	transmission
x_{25}	y_{25}	steel lattice tower	transmission
x_{26}	y_{26}	steel lattice tower	transmission
x_{27}	y_{27}	steel lattice tower	transmission
x_{28}	y_{28}	concrete pole	transmission
x_{29}	y_{29}	concrete pole	distribution
x_{30}	y_{30}	concrete pole	distribution
x_{31}	y_{31}	concrete pole	distribution
x_{32}	y_{32}	concrete pole	distribution
x_{33}	y_{33}	concrete pole	distribution
x_{34}	y_{34}	overhead line	transmission
x_{35}	y_{35}	overhead line	transmission
x_{36}	y_{36}	overhead line	transmission
x_{37}	y_{37}	overhead line	transmission
x_{38}	y_{38}	overhead line	transmission
x_{39}	y_{39}	overhead line	transmission
x_{40}	y_{40}	overhead line	distribution
x_{41}	y_{41}	overhead line	distribution
x_{42}	y_{42}	overhead line	distribution
x_{43}	y_{43}	overhead line	distribution
x_{44}	y_{44}	overhead line	distribution
x_{45}	y_{45}	underground cable	transmission
x_{46}	y_{46}	underground cable	distribution
x_{47}	y_{47}	underground cable	distribution
x_{48}	y_{48}	underground cable	distribution
x_{49}	y_{49}	underground cable	distribution
x_{50}	y_{50}	underground cable	distribution

Table 9

The active and reactive power generation, the active and reactive power demand, and the physical parameters (i.e., the length, resistance, and reactance), of each power grid component (matrix \bar{P}).

Table 10

The number and category of customers connected to each power grid component (matrix $\bar{S} E$).

Table 11

Power grid components exposed to floods of different frequency (matrix \bar{E}).

$$\bar{\bar{\bar{E}}}_{T_{20}} = \begin{bmatrix} \bar{C}_6 \\ \bar{C}_7 \\ \bar{C}_8 \\ \bar{C}_9 \\ \bar{C}_{10} \\ \bar{C}_{11} \\ \bar{C}_{12} \\ C_{13} \end{bmatrix}, \bar{\bar{\bar{E}}}_{T_{50}} = \begin{bmatrix} \bar{C}_6 \\ \bar{C}_7 \\ \bar{C}_8 \\ \bar{C}_9 \\ \bar{C}_{10} \\ \bar{C}_{11} \\ \bar{C}_{12} \\ C_{13} \end{bmatrix}, \bar{\bar{\bar{E}}}_{T_{100}} = \begin{bmatrix} \bar{C}_6 \\ \bar{C}_7 \\ \bar{C}_8 \\ \bar{C}_9 \\ \bar{C}_{10} \\ \bar{C}_{11} \\ \bar{C}_{12} \\ C_{13} \end{bmatrix}, \bar{\bar{\bar{E}}}_{T_{200}} = \begin{bmatrix} \bar{C}_6 \\ \bar{C}_7 \\ \bar{C}_8 \\ \bar{C}_9 \\ \bar{C}_{10} \\ \bar{C}_{11} \\ \bar{C}_{12} \\ C_{13} \end{bmatrix}, \bar{\bar{\bar{E}}}_{T_{500}} = \begin{bmatrix} \bar{C}_1 \\ \bar{C}_6 \\ \bar{C}_7 \\ \bar{C}_8 \\ \bar{C}_9 \\ \bar{C}_{10} \\ \bar{C}_{11} \\ \bar{C}_{12} \\ C_{13} \end{bmatrix}$$

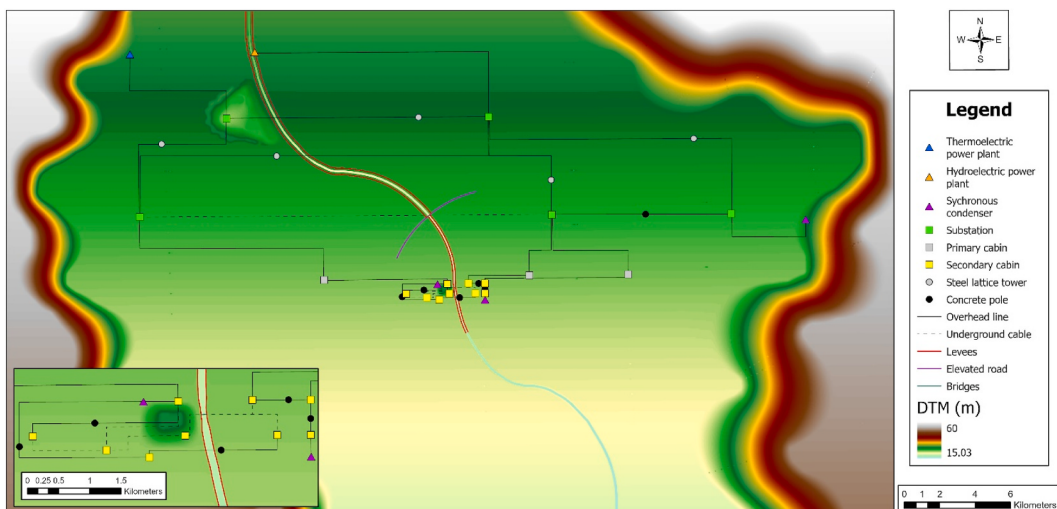


Fig. 11. Digital terrain model (DTM) of the area of interest.

Data availability

Data will be made available on request.

References

- [1] S. Mukherjee, R. Nategi, M. Hastak, A multi-hazard approach to assess severe weather-induced major power outage risks in the U.S, Reliab. Eng. Syst. Saf. 175 (2018) 283–305, <https://doi.org/10.1016/j.ress.2018.03.015>.
- [2] A. Ankit, Z. Liu, S.B. Miles, Y. Choe, U.S. Resilience to large-scale power outages in 2002–2019, J. Saf. Sci. Resil. 3 (2022) 128–135, <https://doi.org/10.1016/j.jnssr.2022.02.002>.
- [3] S.M. Lee, S. Chinthaivali, N. Bhusal, N. Stenvig, T. Kuruganti, Quantifying the power system resilience of the US power grid through weather and power outage data Mapping, IEEE Access 12 (2024) 5237–5255, <https://doi.org/10.1109/ACCESS.2023.3347129>.
- [4] E.E. Koks, K.C.H. Van Ginkel, M.J.E. Van Marle, A. Lemnitzer, Brief Communication: critical Infrastructure impacts of the 2021 mid-July western European flood event, Nat. Hazards Earth Syst. Sci. 22 (2022) 3831–3838, <https://doi.org/10.5194/nhess-22-3831-2022>.
- [5] R. Pant, S. Thacker, J.W. Hall, D. Alderson, S. Barr, Critical infrastructure impact assessment due to flood exposure, J. Flood Risk Manag. 11 (2018) 22–33, <https://doi.org/10.1111/jfr3.12288>.
- [6] L.G. Brunner, R.A.M. Peer, C. Zorn, R. Paulik, T.M. Logan, Understanding cascading risks through real-world interdependent urban infrastructure, Reliab. Eng. Syst. Saf. 241 (2024) 109653, <https://doi.org/10.1016/j.ress.2023.109653>.
- [7] A. Fekete, Critical infrastructure and flood resilience: cascading effects beyond water, WIREs Water 6 (2019) e1370, <https://doi.org/10.1002/wat2.1370>.
- [8] G. Forzieri, A. Bianchi, F. Batista e Silva, M.A. Marin Herrera, A. Leblois, C. Lavalle, J.C.J.H. Aerts, L. Feyen, Escalating impacts of climate extremes on critical infrastructures in Europe, Glob. Environ. Change 48 (2018) 97–107, <https://doi.org/10.1016/j.gloenvcha.2017.11.007>.
- [9] R. Schotten, E. Mühlhofer, G.-A. Chatzistefanou, D. Bachmann, A.S. Chen, E.E. Koks, Data for critical infrastructure network modelling of natural hazard impacts: needs and influence on model characteristics, Res. Cities Struct. 3 (1) (2024) 55–65, <https://doi.org/10.1016/j.rcns.2024.01.002>.
- [10] E. Zio, Challenges in the vulnerability and risk analysis of critical infrastructures, Reliab. Eng. Syst. Saf. 152 (2016) 137–150, <https://doi.org/10.1016/j.ress.2016.02.009>.
- [11] B. Merz, H. Kreibich, R. Schwarze, A. Thielen, Review article "Assessment of economic flood damage", Nat. Hazards Earth Syst. Sci. 10 (2010) 1697–1724, <https://doi.org/10.5194/nhess-10-1697-2010>.
- [12] E. Penning-Roselli, S. Priest, D. Parker, J. Morris, S. Tunstall, C. Viavattene, J. Chatterton, D. Owen, *Flood and Coastal Erosion Risk Management: A Manual for Economic Appraisal*, Routledge, London, 2013. ISBN 978-0-415-81515-4.
- [13] P. Asaridis, D. Molinari, A conceptual model for the estimation of flood damage to power grids, Adv. Geosci. 61 (2023) 1–21, <https://doi.org/10.5194/adgeo-61-1-2023>.
- [14] S. Espinoza, M. Panteli, P. Mancarella, H. Rudnick, Multi-phase assessment and adaptation of power systems resilience to natural hazards, Elec. Power Syst. Res. 136 (2016) 352–361, <https://doi.org/10.1016/j.epsr.2016.03.019>.
- [15] L.A. Bollinger, G.P. Dijkema, Evaluating infrastructure resilience to extreme weather – the case of the Dutch electricity transmission network, Eur. J. Transport Infrastruct. Res. 16 (2016) 214–239, <https://doi.org/10.18757/ejfir.2016.16.1.3122>.
- [16] A. Vasenev, L. Montoya, A. Ceccarelli, A hazus-based method for assessing robustness of electricity supply to critical smart grid consumers during flood events. 2016 11th International Conference on Availability, Reliability and Security (ARES), Salzburg, Austria, 2016, <https://doi.org/10.1109/ARES.2016.12>, 31 August 2016 – 02 September 2016.
- [17] W. Li, E.A.M. Cesena, L.S. Cunningham, M. Panteli, D.M. Schultz, S. Mander, C.K. Gan, P. Mancarella, Assessing power system resilience to floods: a geo-referenced statistical model for substation inundation failures. 2022 IEEE PES Innovative Smart Grid Technologies Conference Europe (ISGT-Europe), 2022, pp. 1–5, <https://doi.org/10.1109/ISGT-Europe54678.2022.9960296>.
- [18] S. Miraei-Ashtiani, F. Vahedifard, M. Karimi-Ghartemani, J. Zhao, I. Mallakpour, A. AghaKouchak, Performance degradation of levee-protected electric power network due to flooding in a changing climate, IEEE Trans. Power Syst. 37 (2022) 4651–4660, <https://doi.org/10.1109/TPWRS.2022.3146229>.
- [19] H. Shahinzadeh, S.M.H. Zanjani, J. Moradi, M. Iranpour, W. Yaici, M. Benbouzid, Resilience assessment of distribution systems against extreme weather events: flooding threats in Iran's electricity network. 2022 Global Energy Conference (GEC), Batman, Turkey, 2022, pp. 247–252. <https://doi.org/10.1109/GEC55014.2022.9987202>.

- [20] S. Afzal, H. Mokhlis, N.N. Mansor, H.A. Illias, J.J. Jamian, M.K.N.M. Sarmin, Modeling and assessing the impact of flash floods on a power distribution system. 2024 IEEE 4th International Conference in Power Engineering Applications (ICPEA), Pulau Pinang, Malaysia, 2024, pp. 322–326, <https://doi.org/10.1109/ICPEA60617.2024.10498988>.
- [21] H.J. Murdock, K.M. de Brujin, B. Gersonius, Assessment of critical infrastructure resilience to flooding using a response curve approach, *Sustainability* 10 (2018) 3470, <https://doi.org/10.3390/su10103470>.
- [22] T. Bragatto, M. Cresta, F. Cortesi, F.M. Gatta, A. Geri, M. Maccioni, M. Paulucci, Assessment and possible solution to increase resilience: flooding threats in terni distribution grid, *Energies* 12 (2019) 744, <https://doi.org/10.3390/en12040744>.
- [23] G.M. Karagiannis, Z.I. Turkezeer, L. Alfrieri, L. Feyen, E. Krausmann, *Climate Change and Critical Infrastructure – Floods*, Publications Office of the European Union, Luxemburg, EUR 28855 EN, 2019.
- [24] E. Koks, R. Pant, S. Thacker, J.W. Hall, Understanding business disruption and economic losses due to electricity failures and flooding, *Int. J. Disaster Risk Sci.* 10 (2019) 421–438, <https://doi.org/10.1007/s13753-019-00236-y>.
- [25] D. Sánchez-Munoz, J.L. Domínguez-García, E. Martínez-Gomariz, B. Russo, J. Stevens, M. Pardo, Electrical grid risk assessment against flooding in Barcelona and Bristol cities, *Sustainability* 12 (2020) 1527, <https://doi.org/10.3390/su12041527>.
- [26] J. Leandro, S. Cunneff, L. Viernstein, Resilience modeling of flood induced electrical distribution network failures: Munich, Germany, *Front. Earth Sci.* 9 (2021) 572925, <https://doi.org/10.3389/feart.2021.572925>.
- [27] X. Deng, S. Friedman, I. Ryan, W. Zhang, G. Dong, H. Rodriguez, F. Yu, W. Huang, A. Nair, G. Luo, S. Lin, The independent and synergistic impacts of power outages and floods on hospital admissions for multiple diseases, *Sci. Total Environ.* 828 (2022) 154305, <https://doi.org/10.1016/j.scitotenv.2022.154305>.
- [28] S. Liasi, N.S. Ghiasi, R. Hadidi, An evaluative framework for regional vulnerability and power system resilience against flooding: a case study of charleston county, South Carolina. 2023 IEEE International Conference on Energy Technologies for Future Grids (ETFG), 2023, pp. 1–6. Wollongong, Australia, <https://10.1109/ETFG55873.2023.10408647>.
- [29] R. Schotten, D. Bachmann, Integrating critical infrastructure networks into flood risk management, *Sustainability* 15 (6) (2023) 5475, <https://doi.org/10.3390/su15065475>.
- [30] E. Mühlhofer, E.E. Koks, C.M. Kropf, G. Sansavini, D.N. Bresch, A generalized natural hazard risk modelling framework for infrastructure failure cascades, *Reliab. Eng. Syst. Saf.* 234 (2023) 109194, <https://doi.org/10.1016/j.ress.2023.109194>.
- [31] Manitoba Hydro International Ltd. <https://www.pscad.com/knowledge-base/article/26>, 2024.
- [32] V.T. Chow, *Open Channel Hydraulics*, MacGraw-Hill, New York, 1959.
- [33] G.W. Brunner, *HEC-RAS River Analysis System: Hydraulic Reference Manual, Version 6.0, CPD-69*, U.S. Army Corps of Engineers, Institute for Water Resources, Hydrologic Engineering Center, Davis, CA, 2021, p. 520.
- [34] G.W. Brunner, Benchmarking of the HEC-RAS Two-Dimensional Hydraulic Modeling Capabilities, US Army Corps of Engineers, Hydrologic Engineering Center, 2020, p. 116.
- [35] S. Terna. <https://www.terna.it/it/sistema-elettrico/codici-rete/codice-rete-italiano>, 2024.
- [36] G. Karagiannakis, M. Panteli, S. Argyroudis, Fragility modeling of power grid infrastructure for addressing climate change risks and adaptation, *WIREs Clim Change* e930 (2024), <https://doi.org/10.1002/wcc.930>.
- [37] S. Nirandjan, E.E. Koks, M. Ye, R. Pant, K.C.H. Van Ginkel, J.C.J.H. Aerts, P.J. Ward, Review article: physical vulnerability database for critical infrastructure hazard risk assessments – a systematic review and data collection, *Nat. Hazards Earth Syst. Sci.* 24 (2024) 4341–4368, <https://doi.org/10.5194/nhess-24-4341-2024>.
- [38] E. Zio, The Monte Carlo simulation method for system Reliability and risk analysis. Springer Series in Reliability Engineering, Springer, London, 2013, p. 198, <https://doi.org/10.1007/978-1-4471-4588-2>.
- [39] M. Chen, T.O. Chan, X. Wang, M. Luo, Y. Lin, H. Huang, Y. Sun, G. Cui, Y. Huang, A risk analysis framework for transmission towers under potential pluvial flood - LiDAR survey and geometric modelling, *Int. J. Disaster Risk Reduct.* 50 (2020) 101862, <https://doi.org/10.1016/j.ijdrr.2020.101862>.
- [40] M. Violante, H. Davani, S.D. Manshadji, A decision support system to enhance electricity grid resilience against flooding disasters, *Water* 14 (2022) 2483, <https://doi.org/10.3390/w14162483>.
- [41] W. Li, L.S. Cunningham, D.M. Schultz, S. Mander, C.K. Gan, M. Panteli, Structural resilience of Pole-mounted substations subjected to flooding: generalized framework and a Malaysian case study, *ASCE-ASME Journal of Risk and Uncertainty in Engineering Systems, Part A: Civ. Eng.* 10 (2) (2024) 04024008, <https://doi.org/10.1061/AJRUA6.RUENG-11>.
- [42] Simulink: R2024a, The MathWorks, Inc., Natick, Massachusetts, United States, 2024. <https://mathworks.com/products/simulink.html>.
- [43] G. Prettico, M.G. Flaminini, N. Andreadou, S. Vitiello, G. Fulli, M. Masera, Distribution System Operators Observatory 2018, Publications Office of the European Union, Luxemburg, 2018. EUR 29615 EN, <https://publications.jrc.ec.europa.eu/repository/handle/JRC113926>.
- [44] S. Terna. <https://www.terna.it/it/sistema-elettrico/statistiche/pubblicazioni-statistiche>, 2024.
- [45] D. Molinari, S. Dazzi, E. Gattai, G. Minucci, G. Pesaro, A. Radice, R. Vacondio, Cost-benefit analysis of flood mitigation measures: a case study employing high-performance hydraulic and damage modelling, *Nat. Hazards* 108 (2021) 3061–3084, <https://doi.org/10.1007/s11069-021-04814-6>.
- [46] S. Thacker, S. Kelly, R. Pant, J.W. Hall, Evaluating the benefits of adaptation of critical infrastructures to hydrometeorological risks, *Risk Anal.* 38 (2018) 134–150, <https://doi.org/10.1111/risa.12839>.
- [47] S. Miraei-Ashtiani, N.L. Dehghani, F. Vahedifard, A. Shafieezadeh, M. Karimi-Ghartermani, Toward equitable grid resilience: operationalizing climate adaptation strategies to mitigate flooding impacts, *Environ. Res.: Infrastruct. Sustain.* 3 (2023) 045009, <https://doi.org/10.1088/2634-4505/ad111e>.
- [48] M. Movahednia, R. Mahroo, A. Kargarian, Transmission-distribution coordination for enhancing grid resiliency against flood hazards, *IEEE Trans. Power Syst.* 39 (3) (2024) 5272–5282, <https://doi.org/10.1109/TPWRS.2023.3325720>.
- [49] S.M. Rinaldi, J.P. Peerenboom, T.K. Kelly, Identifying, understanding, and analyzing critical infrastructure interdependencies, *IEEE Control Syst. Mag.* 21 (2001) 11–25, <https://doi.org/10.1109/37.969131>.
- [50] Dullo, T. T., Darkwah, G. K., Gangrade, S., Morales-Hernández, M., Sharif, M. B., Kalyanapu, A. J., Kao, S.-C., Ghafoor, S., and Ashfaq, M.: Assessing climate-change-induced flood risk in the Conasauga River watershed: an application of ensemble hydrodynamic inundation modeling, *Nat. Hazards Earth Syst. Sci.*, 21, 1739–1757, e-distribuzione S° title="https://doi.org/10.5194/nhess-21-1739-2021, 2021. e-distribuzione S°>https://doi.org/10.5194/nhess-21-1739-2021, 2021. e-distribuzione S.p.A.: https://www.e-distribuzione.it/Azienda/Rete/il-sistema-elettrico.html, last access: 2 October 2024a. e-distribuzione S.p.A.: https://www.e-distribuzione.it/connessione-all-a-rete/Regole_tecniche.html, last access: 2 October 2024b." data-bbox="100 720 920 750">https://doi.org/10.5194/nhess-21-1739-2021, 2021. e-distribuzione S.p.A.: https://www.e-distribuzione.it/Azienda/Rete/il-sistema-elettrico.html, last access: 2 October 2024a. e-distribuzione S.p.A.: https://www.e-distribuzione.it/connessione-all-a-rete/Regole_tecniche.html, last access: 2 October 2024b.
- [51] FEMA: *Hazus Flood Model Technical Manual*, Federal Emergency Management Agency, Washington, D.C., 2022.